HOSTED BY

ELSEVIER

Available online at www.sciencedirect.com

ScienceDirect

Journal of Magnesium and Alloys 5 (2017) 439–447
www.elsevier.com/journals/journal-of-magnesium-and-alloys/2213-9567

Full Length Article

Effects of Mg^{2+} interstitial ion on the properties of $Mg_{0.5+x/2}Si_{2-x}Al_x(PO_4)_3$ ceramic electrolytes

Z.A. Halim [a], S.B.R.S. Adnan [b,*], F.M. Salleh [b], N.S. Mohamed [b]

[a] *Institute of Graduate Studies, University of Malaya, 50603, Kuala Lumpur, Malaysia*
[b] *Centre for Foundation Studies in Science, University of Malaya, 50603, Kuala Lumpur, Malaysia*

Received 30 March 2017; revised 23 August 2017; accepted 29 September 2017

Available online 1 November 2017

Abstract

Nasicon type, $Mg_{0.5+x/2}Si_{2-x}Al_x(PO_4)_3$ was synthesized using citric acid assisted sol-gel method. The X-ray diffraction was applied to investigate the effect of extra Mg^{2+} interstitial ion on the phase, unit cell parameters and structure of the samples. The $Mg_{0.625}Si_{1.75}Al_{0.25}(PO_4)_3$ sample exhibited highest bulk conductivity value of 1.54×10^{-4} S cm^{-1} at ambient temperature. The frequency dependence of the σ_{ac} of these ceramic electrolytes follows the universal power law variation, $\sigma_{ac}(\omega) = \sigma_o + A\omega^{\alpha}$. The conductivity parameters such as hopping frequencies, charge carrier concentration and mobile ion concentration proved that the increase in conductivity with x was due to the existence of Mg^{2+} interstitial ions. The experiment results also revealed that the dielectric constant and dielectric loss decreased with frequency. The $Mg_{0.625}Si_{1.75}Al_{0.25}(PO_4)_3$ was found to be electrochemically stable up to 2.51 V at ambient temperature.

Keywords: Ceramic; Electrolyte; Mg electrolyte; Interstitial ion; Nasicon

1. Introduction

Magnesium batteries have recently attracted great interest due to their high energy density and environmentally friendly components [1]. Theoretically, these Mg batteries can offer high volumetric specific capacity compared to lithium (3833 mAh/cm^3 for Mg vs. 2046 mAh/cm^3 for Li) [1]. Considering all these aspects, it is clear that magnesium battery systems could offer a significantly cheaper, safer and better-performing battery option in contrast to lithium [1]. Despite these attractive attributes of Mg batteries, there are several challenges pertaining to the use of cathodes, electrolytes and anodes. With respect to electrolytes, the magnesium electrolytes' compound has to show high ionic conductivity, large enough interstitial void and high structural stability based on 3D framework [2].

There are only a limited number of works on the use of magnesium as an electrolyte in magnesium batteries. This is due to the (i) difficulty for the divalent Mg-ion to diffuse in solid electrolytes compared to the monovalent Li-ion, (ii) narrow electrical window of electrolytes used for Mg-ion electrochemical activity and finally (iii) relatively low specific energy of magnesium ion batteries compared to its lithium counterpart [3]. Anuar et al started to synthesize magnesium electrolytes based on Nasicon type, $Mg_{0.5}Zr_2(PO_4)_3$ [2]. However, the Nasicon's lattice size was too large making the structure unstable. To overcome this problem, the authors replaced Zr^{4+} with Si^{4+} as reported in an early paper [4] in order to reduce the lattice size of the Nasicon's structure. The conductivity of $Mg_{0.5}Si_2(PO_4)_3$ solid electrolytes is an order of magnitude higher than the $Mg_{0.5}Zr_2(PO_4)_3$ solid electrolytes.

The conductivity of the Nasicon materials can also be improved by modifying their unit cell dimension and ion concentration (interstitial ion and vacant site) [5–7]. Therefore, in the effort to enhance the conductivity of previous $Mg_{0.5}Si_2(PO_4)_3$ compound, the authors substituted Al^{3+} at the Si^{4+} site ($Si^{4+} \leftrightarrow Al^{3+} + 1/2Mg^{2+}$) in order to create Mg^{2+} interstitial ions in the lattice site to obtain compounds with formula $Mg_{0.5+x/2}Si_{2-x}Al_x(PO_4)_3$. To the best of our knowledge, no studies on the use of Al^{3+} as conductivity enhancing agent in the $Mg_{0.5}Si_2(PO_4)_3$ compound have been reported in the literature.

In this paper, the effects of Mg^{2+} interstitial ion on the structural, electrical and electrochemical properties of the $Mg_{0.5+x/2}Si_{2-x}Al_x(PO_4)_3$ compound prepared by the sol-gel method were investigated. For this purpose, the $Mg_{0.5+x/2}Si_{2-x}Al_x(PO_4)_3$

* Corresponding author. Centre for Foundation Studies in Science, University of Malaya, 50603, Kuala Lumpur, Malaysia.
E-mail address: syed_bahari@um.edu.my (S.B.R.S. Adnan).

https://doi.org/10.1016/j.jma.2017.09.005

samples were subjected to X-ray diffraction, scanning electron microscopy, particle size, impedance spectroscopy and linear sweep voltammetry analysis.

2. Experimental procedure

2.1. Synthesis of $Mg_{0.5+x/2}Si_{2-x}Al_x(PO_4)_3$ samples

For sample preparation, magnesium acetate tethrahydrate ($C_4H_6MgO_4{\cdot}4H_2O$), tetraethyl orthosilicate ($SiC_8H_{20}O_4$), aluminum acetate ($C_6H_9AlO_6$) and ammonium phosphate monobasic (H_6NO_4P) were used as the starting materials. Meanwhile citric acid ($C_6H_8O_7$) was employed as the chelating agent. The molar ratio of Mg:Si:Al:P:O was determined based on the stoichiometric formula of $Mg_{0.5+x/2}Si_{2-x}Al_x(PO_4)_3$ with $x = 0.10$, 0.15, 0.20 and 0.25. The starting materials were first dissolved separately in distilled water and then stirred for 1 h under magnetic stirring at a temperature of 30 °C. All of the solutions were mixed together and stirred in a reflux system at 70 °C for 24 h to form a homogeneous solution. The solution was taken out and then evaporated for at least 7 h under magnetic stirring at 80 °C. The resulting wet gel was dried in a vacuum oven at 150 °C for 24 h to remove water particles and organic resistance. The obtained powder was heated at 400 °C for 4 h to remove ammonium and acetate groups. The powders obtained were pressed using a Specac pellet press at 3 tons pressure to form pellets with mass, diameter, thickness, and density of 0.5 g, 13 mm, 2 mm and 1.88 g/cm^{-3}, respectively. Eventually, the samples were later annealed at sintering temperatures of 800 °C for 4 h.

2.2. Characterization techniques

The X-ray powder diffraction analysis was carried out using PANalytical-X'pert^3 X-ray diffractometer with Cu-Kα radiation of wavelength of 1.5406 Å in 2θ range from 10° to 40°. Then, the monoclinic lattice parameters of the samples were calculated using the formula [8]:

$$\frac{1}{d^2} = \frac{1}{\sin^2\beta}\left(\frac{h^2}{a^2} + \frac{k^2\sin^2\beta}{b^2} + \frac{l^2}{c^2} - \frac{2hl\cos\beta}{ac}\right) \quad (1)$$

and

$$d = \frac{\lambda}{2\sin\theta} \quad (2)$$

where d is the distance between crystal planes of *(hkl)*, λ is the X-ray wavelength, θ is the diffraction angle of crystal plane, *hkl* is the crystal index, a, b and c are the lattice parameters and β is the angle between a and c. A Zeiss-Evo MA10 scanning electron microscope was used to conduct morphological analysis of the $Mg_{0.5+x/2}Si_{2-x}Al_x(PO_4)_3$ powders. The particle size information of the ceramic samples was acquired using FRITSCH-Analysette 22 NanoTec laser particle sizer at room temperature. The density (ρ) was also calculated from the mass and sample dimensions using following equations [9,10],

$$\rho = \frac{m}{\pi r^2 t} \quad (3)$$

where m is the mass, r is the radius and t is the thickness of the pallet. Complex impedance parameters (i.e. impedance and phase angle parameters) were measured with a computer-controlled Solatron 1260 impedance analyzer. The samples were sandwiched between platinum electrodes which served as non-blocking electrodes in a frequency range from 0.1 to 10^6 Hz. The total conductivity, σ_t (bulk conductivity, σ_b + grain boundary conductivity, σ_{gb}) which represents the direct current (dc) conductivity in the ceramic sample was calculated using the equation:

$$\frac{1}{\sigma_t} = \frac{1}{\sigma_b} + \frac{1}{\sigma_{gb}} \quad (4)$$

where $\sigma_b = \dfrac{d}{AR_b}$ and $\sigma_{gb} = \dfrac{d}{AR_{gb}}$

In these equations, d is the sample thickness, A is the cross-sectional area of the sample, R_b is the bulk resistance and R_{gb} is the grain boundary resistance. Ac conductivity has been evaluated from dielectric data in accordance with the relation:

$$\sigma_{ac} = \omega\varepsilon_o\varepsilon''\tan\delta \quad (5)$$

where ε_o is the permittivity of the free space (8.854×10^{-14} F cm^{-1}), $\omega = 2\pi f$, ε'' is the dielectric loss and tan δ is the loss tangent factor. The electrochemical stability of the studied samples was evaluated by LSV using Wonatech ZIVE MP2 multichannel electrochemical workstation. The samples were placed between two stainless steel blocking electrodes and a potential current of 0.5 V was applied in order to polarize them. The current was then monitored as a function of time until it reached a steady state condition.

Magnesium transference number measurement was performed using Bruce and Vincent method in order to determine the actual type of charge carriers. The magnesium transference number ($\tau_{Mg^{2+}}$) was calculated using the equation [10,11]:

$$\tau_{Mg^{2+}} = \frac{I_{ss}(\Delta V - I_o R_o)}{I_o(\Delta V - I_{ss}R_{ss})} \quad (6)$$

where I_o is initial current ($t = 0$), I_{ss} is steady state current, R_o and R_{ss} are the initial resistance of the passive layer (before polarization) and the resistance of the passive layer (after polarization) respectively and ΔV is applied voltage bias ($\Delta V = 0.27$V).

3. Result and discussion

Presented in Fig. 1 is the XRD spectra of $Mg_{0.5+x/2}Si_{2-x}Al_x(PO_4)_3$ ($x = 0.10$, 0.15, 0.20 and 0.25) samples. All of the samples exhibit sharp diffraction peaks attributed only to $Mg_{0.5+x/2}Si_{2-x}Al_x(PO_4)_3$ which proves that all compounds were pure. The XRD spectra of the samples were indexed to monoclinic structure with a space group of *P12$_1$/c1*. All of the $Mg_{0.5+x/2}Si_{2-x}Al_x(PO_4)_3$ peaks are sharp and well defined, indicating that the samples are generally well crystallized.

There are synchronizations between the result of lattice parameters, crystallite size, density and volume of the samples which increase with the increase of x as shown in Table 1. The

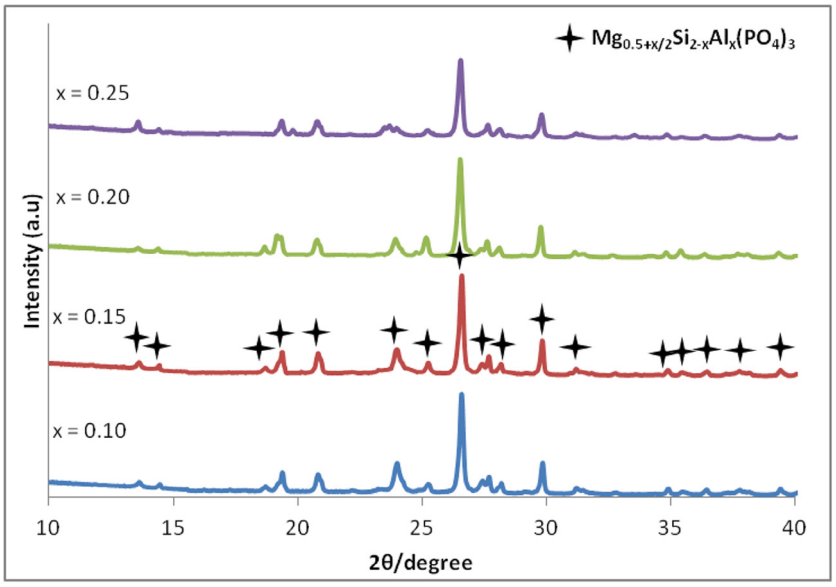

Fig. 1. X-ray diffractograms $Mg_{0.5+x/2}Si_{2-x}Al_x(PO_4)_3$ samples.

increase of Mg-ion interstitial was found to affect the structures of the ceramic compounds. The increase in the unit cell volume is attributed to the larger atomic size of Al^{3+} than Si^{4+} and due to the existence of additional interstitial Mg^{2+} ion after successful partial substituted process in the samples. It is also shown that the density of all compounds have been decreasing after the sintering process. This is because of the thermal shrinkage process in sol-gel method [12]. Meanwhile, the increase in the crystallite size is due to the grain growth process on the samples [13,14].

SEM micrographs and particle size distributions of the $Mg_{0.5+x/2}Si_{2-x}Al_x(PO_4)_3$ ($x = 0.10$, 0.15, 0.20 and 0.25) samples are displayed in Fig. 2 and Fig. 3 respectively. SEM micrographs show that the particle size increases from $x = 0.10$ to $x = 0.25$. Meanwhile, Fig. 3 clearly shows that the size of the particles in $Mg_{0.5+x/2}Si_{2-x}Al_x(PO_4)_3$ samples increases with the increase of x. As the x increases, the average size of the particles in the $Mg_{0.5+x/2}Si_{2-x}Al_x(PO_4)_3$ samples increases from 35.7 μm to 58.9 μm.

The impedance plots of the $Mg_{0.5+x/2}Si_{2-x}Al_x(PO_4)_3$ ($x = 0.10$, 0.15, 0.20 and 0.25) samples are shown in Fig. 4. The impedance plot for every sample consists of two overlapping semicircles with a titled spike at low frequency region. The high frequency semicircle is ascribed to bulk response with its intercept at the x-axis attributed to bulk resistance, R_b, while the middle frequency semicircle is associated to grain boundary response with its intercept at the x-axis corresponding to grain boundary resistance, R_{gb} [15]. On the other hand, the spike that can be clearly seen at the low frequency region of the spectra indicates the effects of electrode polarization as a result of accumulation of ions between electrode and samples [16].

The complex impedance data obtained experimentally for the $Mg_{0.5+x/2}Si_{2-x}Al_x(PO_4)_3$ ($x = 0.10$, 0.15, 0.20 and 0.25) samples at room temperature may be approximately denoted by the impedance of an equivalent circuit consisting of bulk resistance (R_b), grain boundary resistance (R_{gb}), bulk, C_b (CPE), grain boundary capacitance C_{gb} (CPE) and CPE blocking electrode as shown in Fig. 5. Table 2 lists direct current conductivity values of all $Mg_{0.5+x/2}Si_{2-x}Al_x(PO_4)_3$ samples calculated using Eq. (3). The conductivity increases consistently from $x = 0.10$ to $x = 0.25$. The sample with $x = 0.25$ gives the highest bulk conductivity with value of 1.54×10^{-4} S cm^{-1} at ambient temperature which is an order of magnitude higher compared to that of the parent compound, $Mg_{0.5}Si_2(PO_4)_3$ as reported in reference [4]. This demonstrates that insertion of Al^{3+} slightly increases the conductivity of this compound by producing additional interstitial Mg^{2+} which increases the number and mobility of ions.

Fig. 6 presents the graph of *log σ(ac)* versus *log ω* for the $Mg_{0.5+x/2}Si_{2-x}Al_x(PO_4)_3$ ($x = 0.10$, 0.15, 0.20 and 0.25) samples. The plot can be divided into three regions; the low frequency, intermediate frequency and high frequency regions. The spectra exhibit a spike in low frequency region due to the polarization effects where the blocking of ions between the sample and electrode occurs. There is a plateau at the intermediate frequency region and extrapolating it to the y-axis gives the value of direct current conductivity, σ_{dc} [17,18]. In this region, the conductivity is frequency independent and the σ_{dc} values are found to be in good agreement with the values listed in Table 2.

Table 1
Lattice parameters, unit cell volume, crystallite size and density of $Mg_{0.5+x/2}Si_{2-x}Al_x(PO_4)_3$ samples.

Samples	a(Å)	b (Å)	c (Å)	V (Å^3)	Crystallite size (Å)	Density (gcm^{-3})
$x = 0.10$	6.707	5.750	12.433	479.496	86.299	1.412
$x = 0.15$	6.720	5.755	12.456	481.687	115.100	1.410
$x = 0.20$	6.733	5.764	12.501	485.172	115.100	1.411
$x = 0.25$	6.740	5.774	12.524	487.327	138.099	1.410

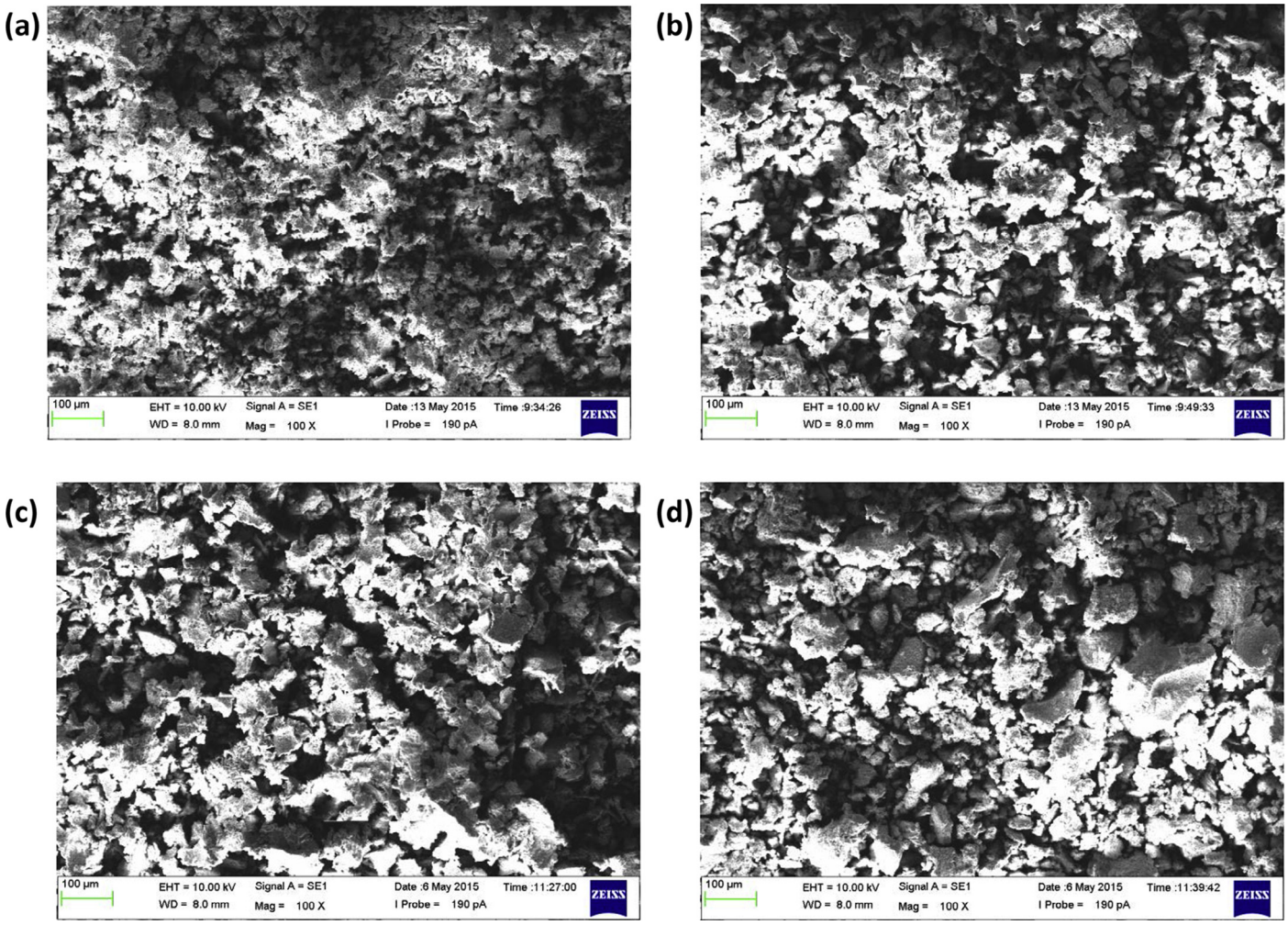

Fig. 2. Cross-sectional SEM micrographs of the $Mg_{0.5+x/2}Si_{2-x}Al_x(PO_4)_3$ samples with (a) $x = 0.10$, (b) $x = 0.15$, (c) $x = 0.20$ and (d) $x = 0.25$.

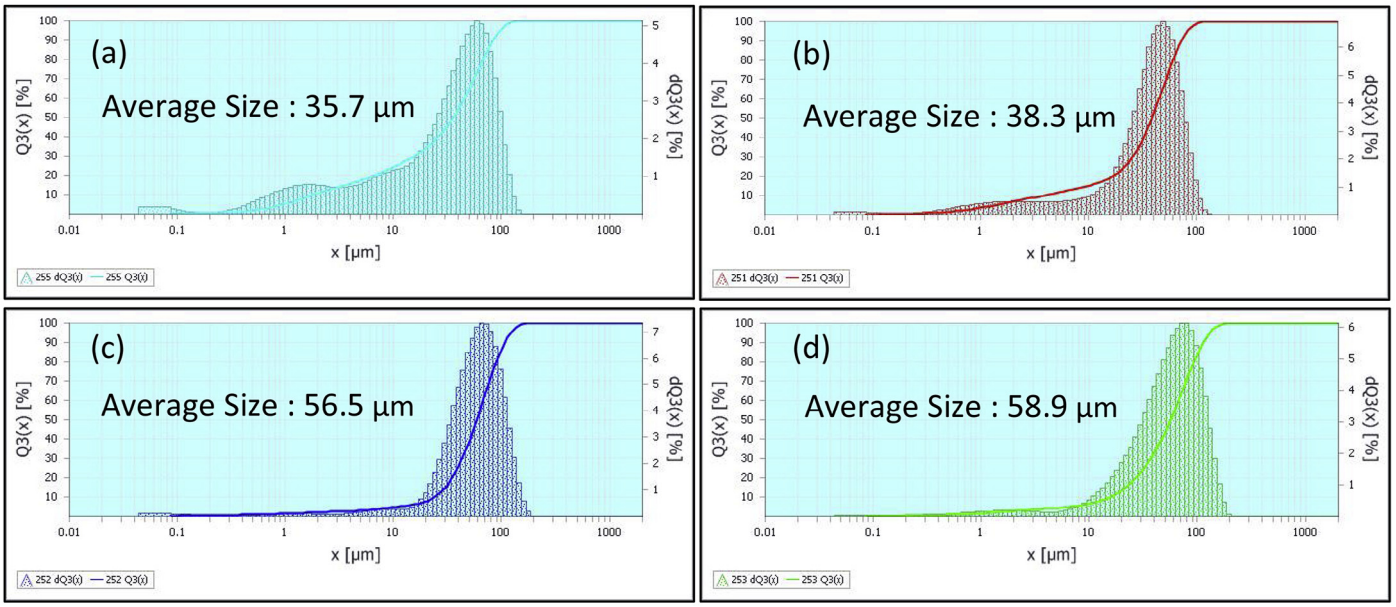

Fig. 3. Particle size distribution of the $Mg_{0.5+x/2}Si_{2-x}Al_x(PO_4)_3$ samples with (a) $x = 0.10$, (b) $x = 0.15$, (c) $x = 0.20$ and (d) $x = 0.25$.

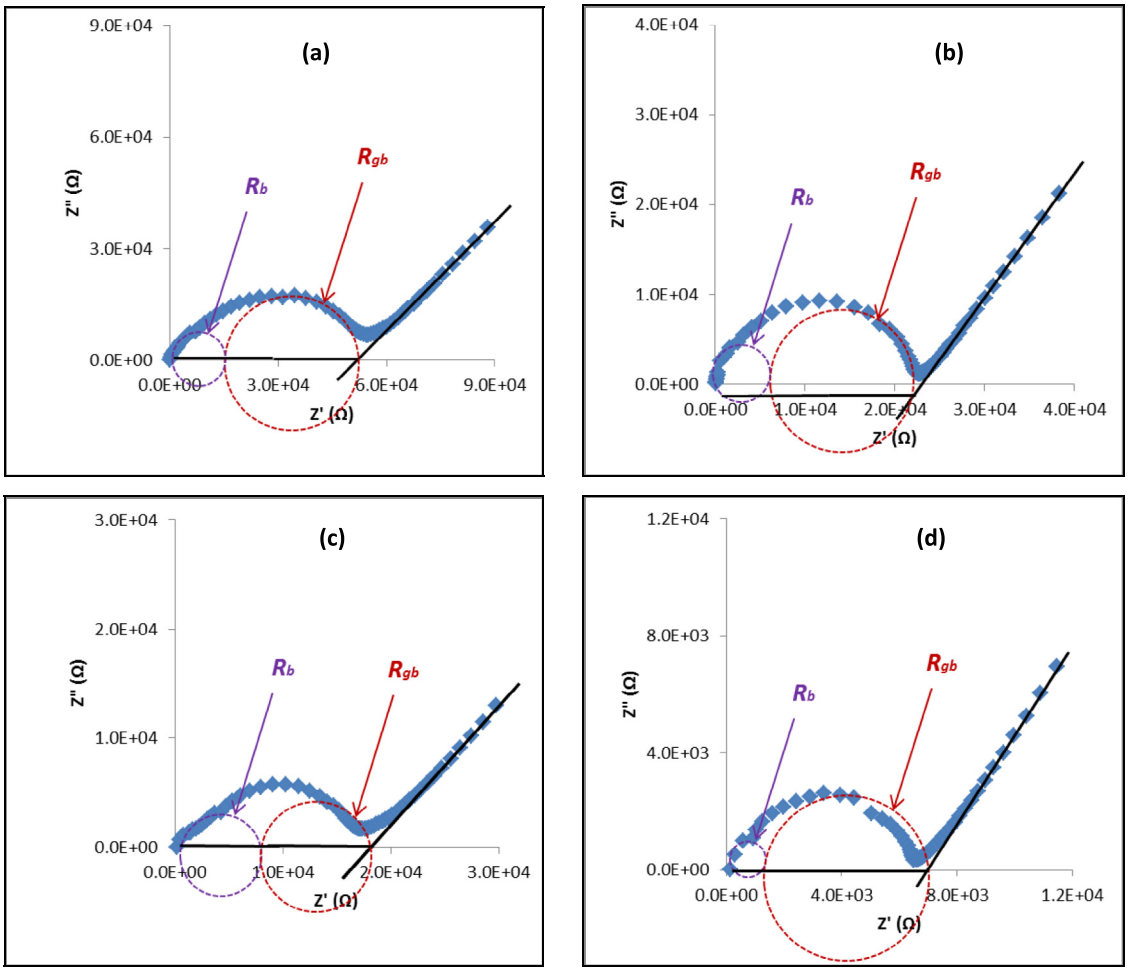

Fig. 4. Typical complex impedance plots of the $Mg_{0.5+x/2}Si_{2-x}Al_x(PO_4)_3$ samples with (a) $x = 0.10$, (b) $x = 0.15$, (c) $x = 0.20$ and (d) $x = 0.25$.

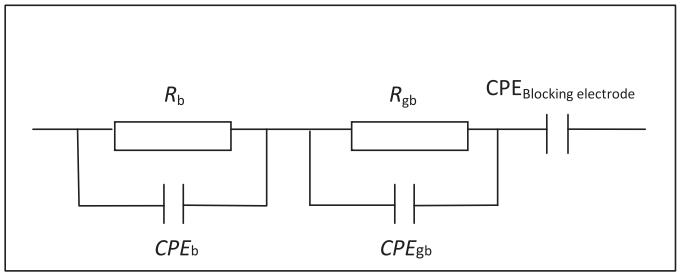

Fig. 5. Equivalent circuit of $Mg_{0.5+x/2}Si_{2-x}Al_x(PO_4)_3$ samples based on the impedance analysis of the samples at room temperature.

Table 2
The σ_b, σ_{gb} and σ_t of $Mg_{0.5+x/2}Si_{2-x}Al_x(PO_4)_3$ samples at ambient temperature.

Sample	x	σ_b (S cm^{-1})	σ_{gb} (S cm^{-1})	σ_t (S cm^{-1})
$Mg_{0.5+x/2}Si_{2-x}Al_x(PO_4)_3$	0.10	1.27×10^{-5}	5.11×10^{-6}	3.65×10^{-6}
	0.15	2.94×10^{-5}	1.17×10^{-5}	8.37×10^{-6}
	0.20	2.52×10^{-5}	1.86×10^{-5}	1.07×10^{-5}
	0.25	1.54×10^{-4}	3.39×10^{-5}	2.78×10^{-5}

On the other hand, at high frequency region, the transition from direct current plateau to alternate current conductivity dispersion occurs.

According Almond and co-workers [19], the ionic hopping ω_p can be directly obtained from alternate current conductivity graph. The value of ionic hopping ω_p can be obtained by extrapolating, at twice the value of direct current conductivity, from the vertical axis horizontally toward the graph and then extrapolating downwards vertical to the horizontal axis as shown in Fig. 6. Using the ω_p value, the magnitude of the charge carrier concentration, K can be calculated using the equation as follows [20,21]:

$$K = \frac{\sigma T}{\omega_p} \tag{7}$$

$$K = ne^2a^2\gamma k^{-1} \tag{8}$$

where e is electron charge, γ is correlation factor which is set equal to 1, and a is the jump distance between two adjacent sites for the ions to hop that is assumed to be 3 Å [22]. The density of mobile ions (Mg^{2+}), n, can be determined using Eq. (8), and

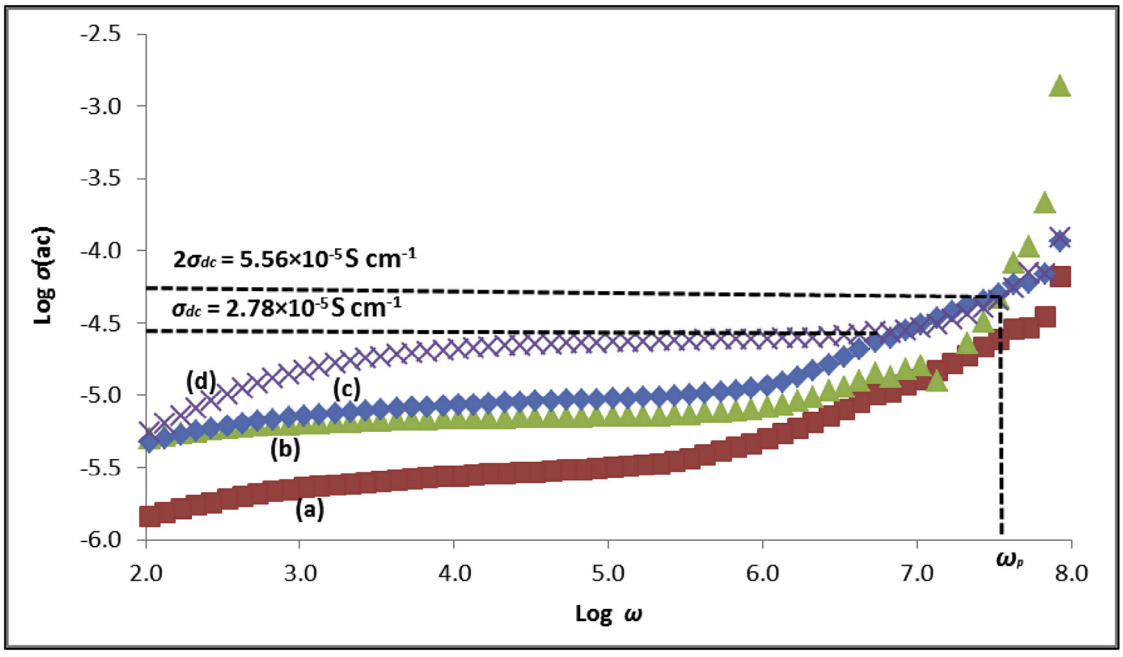

Fig. 6. Alternate current conductivity spectra of the $Mg_{0.5+x/2}Si_{2-x}Al_x(PO_4)_3$ samples with (a) $x = 0.10$, (b) $x = 0.15$, (c) $x = 0.20$ and (d) $x = 0.25$.

k is the Boltzmann constant. The ionic mobility, μ can be evaluated using Eq. (9):

$$\mu = \frac{\sigma_{dc}}{ne} \tag{9}$$

The values of ω_p, K, n and μ at room temperature studied for $Mg_{0.5+x/2}Si_{2-x}Al_x(PO_4)_3$ compounds are presented in Table 3. The values of ω_p, K, n and μ increase with the increase in x. This means that the rise in conductivity in the samples can be attributed to the extra Mg^{2+} interstitial ion which rises in ionic mobility as well as density of mobile ions [22–24].

Fig. 7 depicts the dielectric constant (ε') versus log f for different x value of $Mg_{0.5+x/2}Si_{2-x}Al_x(PO_4)_3$ samples. At low frequency region, the value of ε' increases with the increase of x. This is due to the contribution of charge carrier accumulation at the interface of the sample and electrode [19–22]. This ε' value is greater than the value in parent compound, $Mg_{0.5}Si_2(PO_4)_3$ as reported in reference [4]. It is proving that, the substitutions of Al^{3+} at the Si^{4+} lattice site ($Si^{4+} \leftrightarrow Al^{3+} + 1/2Mg^{2+}$) affected the number of charge carrier in the sample.

Fig. 8 shows the graph of dielectric loss (ε'') of $Mg_{0.5+x/2}Si_{2-x}Al_x(PO_4)_3$ as a function of log f at different value of x. The ε'' values also increase with the increase of x at low frequency region. It's because, when the x value increases, the large amount of Mg^{2+} interstitial ions is created. The increase of Mg^{2+} interstitial ions results in high electrical energy loss due to the migration of ion to the surface of the sample which increases the value of ε'' [22–25].

Fig. 9 presents the plot of frequency dependence of tan $\delta = \varepsilon''/\varepsilon'$ at different x. The plot shows a peaking behavior for all x. As the x increases, the tan δ peaks are shifted toward higher frequency. The angular frequency ω ($\omega = 2\pi f_{max}$) which

Table 3
Value of ω_p, K, n and μ at room temperatures for $Mg_{0.5+x/2}Si_{2-x}Al_x(PO_4)_3$ samples.

Sample	ω_p (Hz)	K (S cm^{-1} K Hz^{-1})	$n \times 10^{23}$ (cm^{-3})	μ (cm^2 V^{-1} s^{-1})
$x = 0.10$	2.69×10^6	4.11×10^{-10}	1.54	1.48×10^{-10}
$x = 0.15$	3.39×10^6	7.48×10^{-10}	2.80	1.87×10^{-10}
$x = 0.20$	4.27×10^6	7.60×10^{-10}	2.84	2.35×10^{-10}
$x = 0.25$	2.27×10^7	7.97×10^{-10}	7.39	2.35×10^{-09}

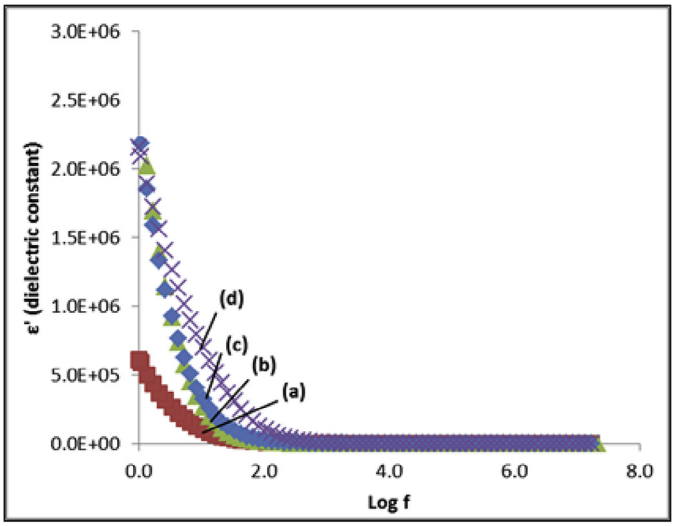

Fig. 7. Plot of dielectric constant (ε') as a function of log f of the $Mg_{0.5+x/2}Si_{2-x}Al_x(PO_4)_3$ samples with (a) $x = 0.10$, (b) $x = 0.15$, (c) $x = 0.20$ and (d) $x = 0.25$.

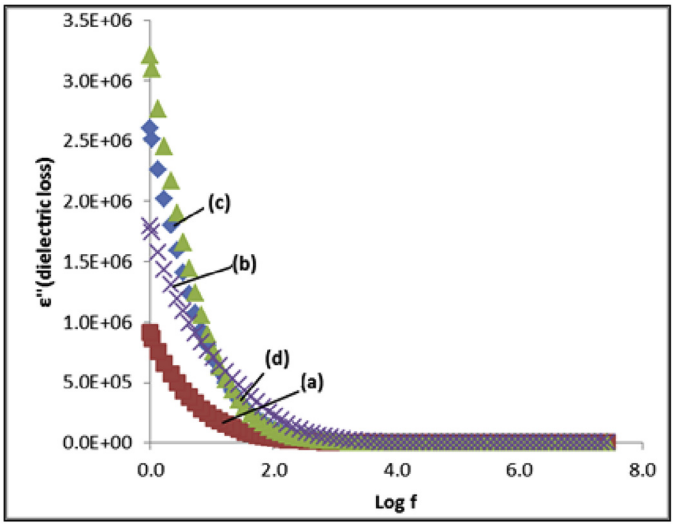

Fig. 8. Plot of dielectric loss (ε'') as a function of log f for the $Mg_{0.5+x/2}Si_{2-x}Al_x(PO_4)_3$ samples with (a) $x = 0.10$, (b) $x = 0.15$, (c) $x = 0.20$ and (d) $x = 0.25$.

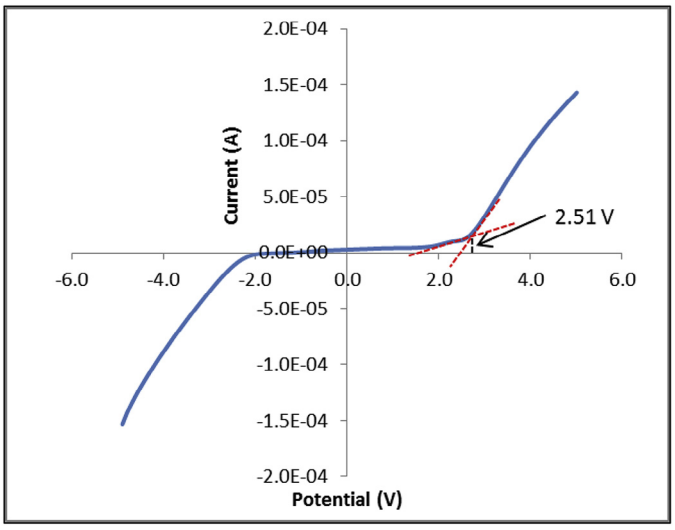

Fig. 10. Linear sweep voltammogram of the $Mg_{0.5+x/2}Si_{2-x}Al_x(PO_4)_3$ samples with $x = 0.25$ with a sweep rate of 50 mV s^{-1}.

corresponds to maximum tan δ gives the relaxation times τ, from the relation [24,25].

$$\omega_{max}\tau = 1 \tag{10}$$

The relaxation times, τ is inversely proportional to jumping probability P which is expressed as [24,25]:

$$\tau = \frac{1}{2}P \tag{11}$$

The τ for the samples with $x = 0.10$, 0.15, 0.20 and 0.25 are 1.71×10^3, 2.15×10^3, 4.28×10^3 and 4.28×10^4 Hz respectively. The results demonstrate that the ions in the sample $x = 0.25$ had the highest jumping probability. This value is higher compared to the τ value in parent compound, $Mg_{0.5}Si_2(PO_4)_3$ (3.8×10^4 Hz) as reported in reference [4]. Its demostrated extra Mg^{2+} interstitial ion affected the jumping probability of ions in the sample.

Linear sweep voltammetry was employed in this work to examine the decomposition voltage of the $Mg_{0.5+x/2}Si_{2-x}Al_x(PO_4)_3$ electrolyte samples. The linear sweep voltammogram of the $Mg_{0.5+x/2}Si_{2-x}Al_x(PO_4)_3$ sample with $x = 0.25$, which is the highest conducting compound is shown in Fig. 10. The value of voltage stability window of the magnesium electrolyte is found to be 2.51 V. This value is acceptable in magnesium battery system since the standard electrode potential between magnesium metal is less than 2.37 V [26].

Meanwhile Fig. 11 shows the plot of current vs. time for $Mg/Mg_{0.625}Si_{1.75}Al_{0.25}(PO_4)_3/Mg$ cell used for the magnesium transference number determination. Under a dc polarization of 0.27 V, the current in the both cells exhibits only a small decay with time. The initial and final steady current for the

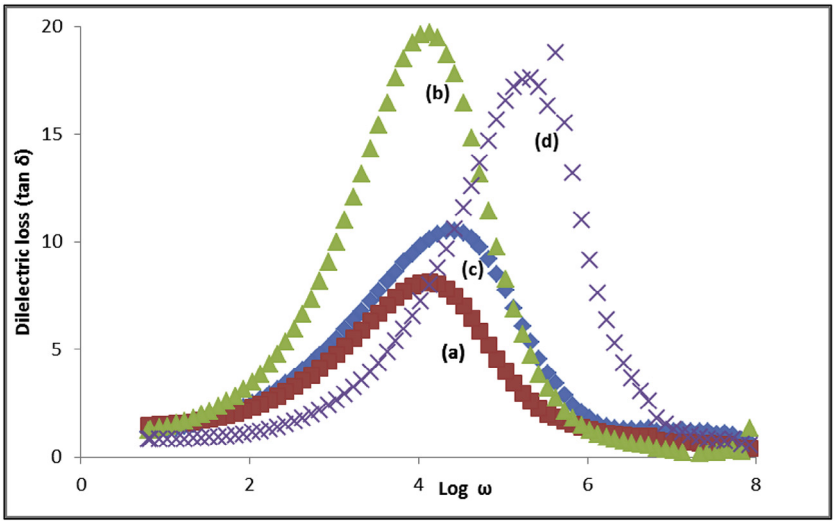

Fig. 9. Frequency dependence of tan δ for the $Mg_{0.5+x/2}Si_{2-x}Al_x(PO_4)_3$ samples with (a) $x = 0.10$, (b) $x = 0.15$, (c) $x = 0.20$ and (d) $x = 0.25$.

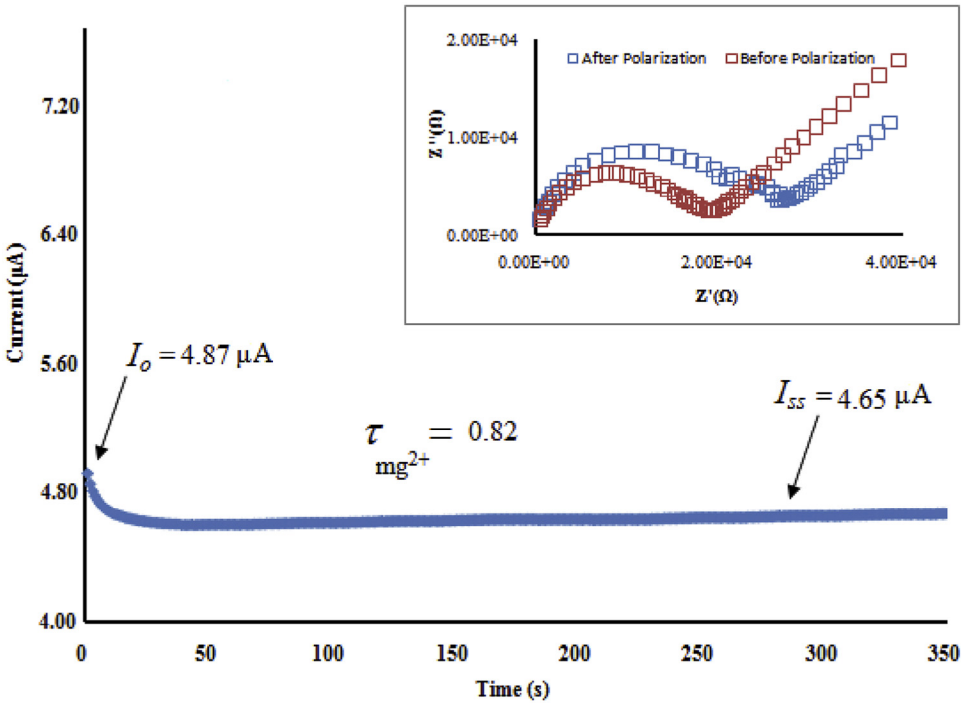

Fig. 11. Plot of current vs. time for $Mg_{0.625}Si_{1.75}Al_{0.25}(PO_4)_3$ compound.

Mg/$Mg_{0.625}Si_{1.75}Al_{0.25}(PO_4)_3$/Mg cell are $I_o = 4.87 \times 10^{-6}$ A and $I_{ss} = 4.65 \times 10^{-6}$ A respectively. The impedance responses of the cells prior to and after polarization for the Mg/$Mg_{0.625}Si_{1.75}Al_{0.25}(PO_4)_3$/Mg cell are $R_o = 20{,}000\ \Omega$ and $R_{ss} = 29{,}000\ \Omega$ respectively. The value magnesium transfer number for $Mg_{0.625}Si_{1.75}Al_{0.25}(PO_4)_3$ compound is 0.82 and confirmed the prepared compound was ionic.

4. Conclusion

The effects of Mg^{2+} interstitial ion on the properties of $Mg_{0.5+x/2}Si_{2-x}Al_x(PO_4)_3$ ceramic electrolytes were studied. The structure of the parent compound was affected by substitution of Al^{3+} and the increase of the Mg^{2+} interstitial ion. Meanwhile, the conductivity study on room temperature showed an increasing pattern up to 1.54×10^{-4} S cm^{-1}. The conductivity parameters such as hopping frequencies, charge carrier concentration and mobile ion concentration proved that the increase in conductivity with x was due to the increase of the Mg^{2+} interstitial ion. The $Mg_{0.625}Si_{1.75}Al_{0.25}(PO_4)_3$ sample exhibited a stable voltage window in voltage range of 2.51 V at ambient temperature. The value of magnesium transference number for the $Mg_{0.625}Si_{1.75}Al_{0.25}(PO_4)_3$ sample was confirmed that the compound was ionic.

Acknowledgement

The authors would like to extend their gratitude toward the University of Malaya and Ministry of Education for funding this work through the Fundamental Research Grant Scheme (project no: FP006-2013B), University of Malaya Research Grant (project no: RP013A-13AFR), and Postgraduate Research Grant (project no: PG032- 2015A).

References

[1] L. Dongping, X. Terrence, S. Partha, M.K. Datta, M.L. Gordin, A. Manivannan, et al., J. Electrochem. Soc. 160 (2) (2013) A351–A355.
[2] N. Anuar, S.B.R.S. Adnan, N.S. Mohamed, Ceram. Int. 40 (2014) 13719–13727.
[3] E. Levi, M. Levi, O. Chasid, D. Aurbach, J. Electroceram. 22 (2009) 13–19.
[4] Z.A. Halim, S.B.R.S. Adnan, N.S. Mohamed, Ceram. Int. 42 (2016) 4452–4461.
[5] Z. Khakpour, Electrochim. Acta 196 (2016) 337–347.
[6] M. Illbeigi, A. Fazlali, M. Kazazi, A.H. Mohammadi, Solid State Ionics 289 (2016) 180–187.
[7] S.B.R.S. Adnan, F.M. Salleh, N.S. Mohamed, Ceram. Int. 42 (15) (2016) 17941–17945.
[8] S.B.R.S. Adnan, N.S. Mohamed, Ceram. Int. 40 (2014) 6373–6379.
[9] T. Rahman, M. Vargas, C.V. Rama, J. Alloys Compd. 617 (2014) 547–562.
[10] N.K. Anuar, S.B.R.S. Adnan, M.H. Jaafar, N.S. Mohamed, Ionics 22 (2016) 1125–1133.
[11] P.G. Bruce, J. Evans, C.A. Vincent, Solid State Ionics 28–30 (1998) 918–922.
[12] X. Wu, Z. Wen, X. Xu, X. Wang, J. Lin, J Nucl Mater 392 (2009) 471–475.
[13] F. Wang, Y. Han, C.S. Lim, Y. Lu, J. Wang, J. Xu, et al., Nature 463 (2010) 1061–1065.
[14] C. Xu, J. Tamaki, N. Miura, N. Yamazoe, Sens. Actuators B Chem. 3 (1991) 147–155.
[15] R. Norhaniza, R. Subban, N.S. Mohamed, J. Mater. Sci. 46 (2011) 7815–7821.
[16] C. Mariappan, G. Govindaraj, Solid state ionics 176 (2005) 1311–1318.
[17] E. Traversa, H. Aono, Y. Sadaoka, L. Montanaro, Sens. Actuators B Chem. 65 (2000) 204–208.
[18] A. Orliukas, A. Dindune, Z. Kanepe, J. Ronis, B. Bagdonas, A. Kežionis, Electrochim. Acta 51 (2006) 6194–6198.
[19] D. Almond, G. Duncan, A. West, Solid State Ionics 8 (1983) 159–164.

[20] R. Sobiestianskas, A. Dindune, Z. Kanepe, J. Ronis, A. Kežionis, E. Kazakevičius, et al., Materials Sci and Eng: B 76 (2000) 184–192.
[21] M. Prabu, S. Selvasekarapandian, A. Kulkarni, G. Hirankumar, A. Sakunthala, Ionics 16 (2010) 317–321.
[22] S.B.R.S. Adnan, N.S. Mohamed, Materials Research Innovations 16 (2012) 281–285.
[23] N. Hegab, A. Bekheet, M. Afifi, L. Wahaba, H. Shehata, Journal Ovonic Research 3 (2007) 71–82.
[24] M. Vijayakumar, G. Hirankumar, M. Bhuvaneswari, S. Selvasekarapandian, J. Power Sources 117 (2003) 143–147.
[25] S.B.R.S. Adnan, N.S. Mohamed, International Journal of Electrochemical Science, International Journal of Electrochemical Science 7 (2012) 9844–9858.
[26] R. Mohtadi, F. Mizuno, Beilstein Journal of Nanotechnology 5 (2014) 1291–1311.